日本医放会誌：50（5），539—547，1990（平2）

Detectability of Simulated Vessels by Computed Radiography and Digital Fluorography

Wataru Misumi, Yoshiharu Higashida[1], Senya Yoshioka[2], Yukunori Korogi[2] and Mutsumasa Takahashi[2]

Kumamoto University Honjo Radioisotope Laboratory

[1]Department of Radiological Technology, College of Medical Science, Kumamoto University

[2]Department of Radiology, Kumamoto University School of Medicine

Research Code No. : 200, 208.1

Key Words : Computed radiography, Digital subtraction angiography, C-D diagram, Detectability, Image processing

CRDSA と DFDSA による模擬血管の検出能

熊本大学医学部本荘 RI 研

1）熊本大学医療技術短期大学部診療放射線技術学科

2）熊本大学医学部放射線医学教室

三隅　凌　東田　善治[1]　吉岡　仙弥[2]

興梠　征典[2]　高橋　睦正[2]

（平成元年5月25日受付）

（平成元年10月26日最終原稿受付）

Computed Radiography（CR）と Digital Fluorography（DF）装置による DSA（Digital Subtraction Angiography）像の検出能について，模擬血管像を用いて検討した．また CRDSA 像の検出能と X 線入射線量，およびコントラスト強調による検出能の改善について検討した．DFDSA による模擬血管の検出能は，CRDSA に比べて優れている．CRDSA による検出能は，入射線量によって影響を受ける．コントラスト強調によって模擬血管の検出能は改善されるが，改善の割合は入射線量，および血管サイズに依存する．

Introduction

Fuji computed radiography (CR) system is a new type of digital radiography systems in which photostimulable phosphors are used as the detector materials for imaging[1]. The CR systems have been used widely in clinical practice as a new modality which has a potential of replacing the conventional screen-film system[2)~5)]. In addition, the CR system is often used as a technique for obtaining the digital subtraction angiographic (DSA) image because of the larger area of imaging plate (IP) used as the detector[6)~10)]. There have been some reports which describe clinical applications of CR in DSA (CRDSA) as a method of evaluating vascular abnomalities[6)~10)]. However, detectability of vessels in CRDSA, influenced by imaging parameters and image processing, remains to be explored quantitatively.

In this study, detectability of the simulated essels was evaluated experimentally in CRDSA in relation

to the incident x-ray exposures and overall contrast enhancement. The experimental results were compared with those of DSA using a DF system (DFDSA). Detectability of the simulated vessels was determined by observer performance experiments.

Materials and Methods

(1) Equipments

The CR system used in this study is a Fuji CR system (CR201, Fuji Photo Film Company, Japan). Its basic components consist of an imaging plate (IP), an image reader, an image processor and an image recorder. The specifications of the system have been reported elsewhere[1].

The DF system (DFA-2, Hitachi Medical Corp. Japan), employed for comparison with the CR system, has an image intensifier (II)-TV system which has been reported in detail elsewhere[11].

(2) Phantom

A contrast-detail (C-D) phantom was produced accoding to the method of Ref. 12. Simulated vessels used for this phantom were approximately 1-cm-length Teflon tubes into which contrast medium, Urografin-76: Sodium and Meglumine Diatrizoate, was injected, and both ends of the tubes were sealed with glue (Chemgrip, Chemplast, New Jersey).

The inside diameters of each tube were 2.69, 1.68, 1.35, 0.96, 0.66, and 0.46 mm. The contrast medium was diluted by distilled water and the concentrations of the contrast medium were varied in eleven levels by a factor of $\sqrt{2}$ from 100% (370 mg/cm^3 of iodine) to 3.1%. The corresponding iodine content at the vessel diameter thus ranged from 99.5 (0.269 cm $\times$ 370 mg/cm^3) to 0.53 mg/cm^2. These tubes were glued to a Lucite plate (2 mm in thickness), each at slightly different angles. This Lucite plate was glued to a plastic case (15.4 cm $\times$ 15.4 cm $\times$ 2.9 cm), which was then filled with 2.8% contrast medium in order to eliminate the effects of the walls of the tubes. A schematic diagram of the C-D phanton is shown in Fig. 1.

(3) CRDSA

Test images were obtained by exposing the C-D phantom on the top of an uniform Lucite block (30 cm $\times$ 30 cm in area and 15 cm in thickness). An antiscatter grid with 40 lines/cm and a 12 to 1 ratio (interspacer: aluminum) was used. The distance between the focal spot and the IP, whose standard type (ST) was employed in this study, was 100 cm and the field size at the IP surface was 35.6 cm $\times$ 35.6 cm (14 inches $\times$ 14 inches). A tube voltage of 75 kV was employed. An x-ray generator (Toshiba KXO-1000) and an x-ray tube (Toshiba Circlex DRX-431HD) with the nominal focal spot size of 2.0 mm were used. The x-ray exposures incident on the IP were measured accurately by using an ionization chamber (Victreen 500) mounted in the fixed position between the focal spot and the IP. The x-ray exposures incident to the IP

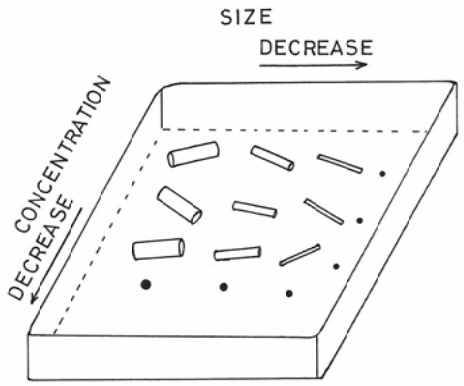

Fig. 1 Schematic diagnram of the C-D phantom.

were varied by changing the tube current and the exposure time. The incident exposures were from 0.3 to 8 mR/image (0.3, 1.4, and 8 mR). All test images were digitized with a 0.2 mm × 0.2 mm aperture (5 pixels/mm in sampling rate), and final images for the CR system were printed on 17.6 cm × 17.6 cm single emulsion films.

Overall contrast enhancement was used as an image processing technique because of its simplicity and of its wide-spread use in digital radiography. Test images with three different contrast enhancement factors (γ=2, 4 and 8) were generated by changing the overall contrast of the original test images (γ=1), the gradient of which was equivalent to that of a radiographic film (Sakura A).

(4) DFDSA

Similar experiments were performed on the DF system to compare the detectablity of the simulated vessels with CR images. DSA images of the C-D phantom were obtained with the use of the serial mode with summation of four frames at 75 kV. Incident dose on the grid in front of the image intensifier (II) were varied from 0.2 to 10 mR/image (0.2, 1, 3.4, and 10 mR).

In the experiments of the DF system, a carbon fiber reinforced plastic (CFRP) grid with 28 lines/cm and an 8 to 1 ratio (interspacer: wood) was used. The field size of the II was 9 inches, and the matrix size was 512 × 512. The window level and window width were selected subjectively for each image to yield an "optimal" appearance of simulated vessles. Finally, all subtracted images of the C-D phantom for the DF system were printed on films for evaluation.

(5) Observer performance studies

Four test images were prepared for all experiments. The detectability of simulated vessels in these images was quantified by means of observer performance studies, in which a contrast-detail (C-D) diagram method was employed[13)~15)]; each observer was asked 1) to select, for each object size, the lowest contrast that is detectable with a 50% confidence level, and 2) to report fractional numbers, if necessary, between adjacent contrasts in order to convey the best estimate of the threshold contrast. The viewing conditions-viewing distance, viewing time, room lighting-were determined by each observer. Each set of test images

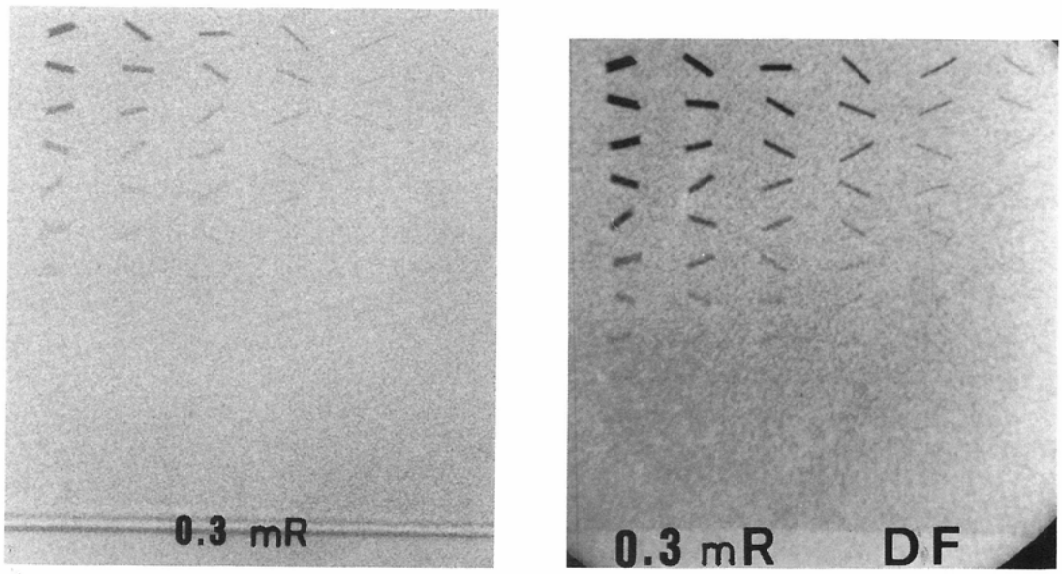

2a　　2b

Fig. 2　Subtracted images of the C-D phantom obtained with the CR (a) and the DF systems at incident exposure of 0.3 mR exposed at 75 kV with a 15-cm-thick Lucite block.

was viewed twice by ten observers and the results were averaged. The experimental procedures and method of data analysis were discussed in detaill elsewhere[16].

Results

(1) Subtracted images of a C-D phantom, obtained with the CR (a) and the DF (b) systems at incident exposure of 0.3 mR are shown in Fig. 2, respectively.

Fig. 3 shows the comparison of simulted vessles, obtained with CR system, before and after contrast

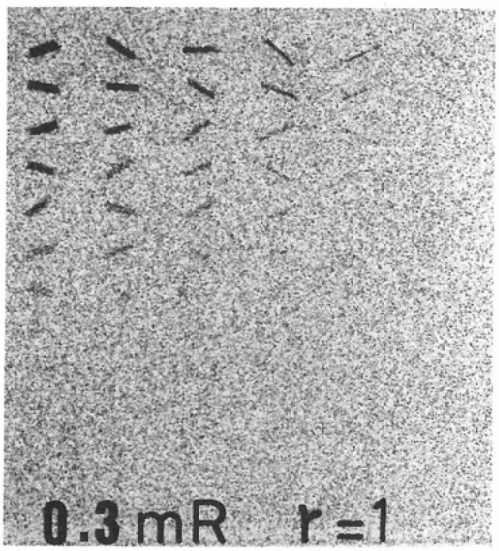

3a-1

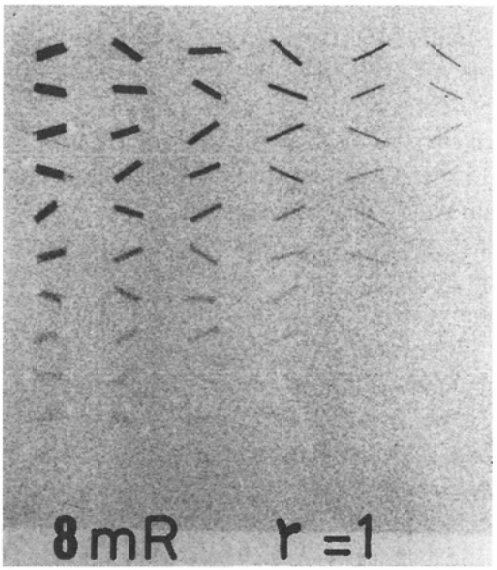

3b-1

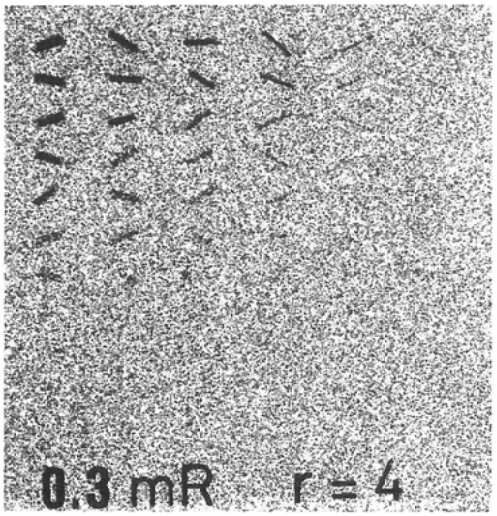

3a-2

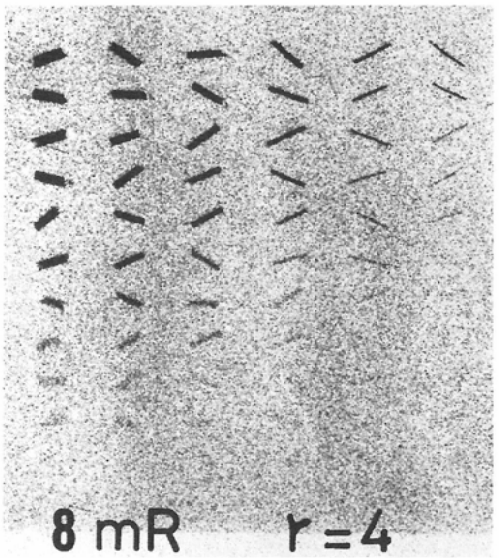

3b-2

Fig. 3 Comparison of simulated vessels before and after contrast enhancement, by a factor of four. (a) incident exposure: 0.3 mR, (b) incident exposure: 8 mR.

enhancement by a factor of 4. It is obvious that the effect of image processing are demonstrated more clearly in the images obtained with high exposure condition (Fig. 3b) than in the images of low exposure condition (Fig. 3a). In each column, the concentration of the contrast medium decreases from the top to the bottom and in each row, the inside diameter of the Teflon tubes decreases from the left to the right. It is obvious that the presence of noise in the images increases with decrease of the incident exposure.

(2) The C-D diagrams without and with overall contrast enhancement (γ=4) are demonstrated for

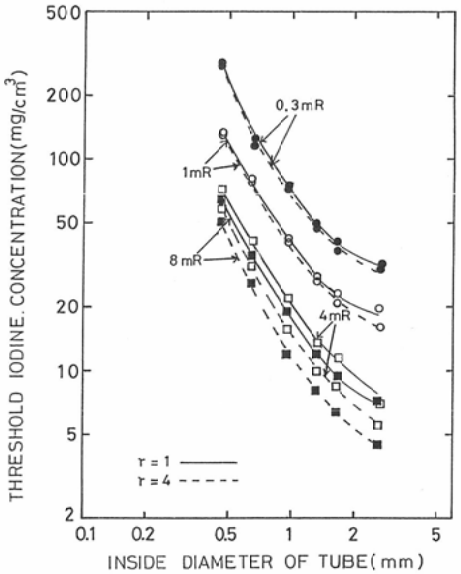

Fig. 4 C-D diagrams without and with overall contrast enhancement (γ=4) obtained with the CR system for various incident exposures.

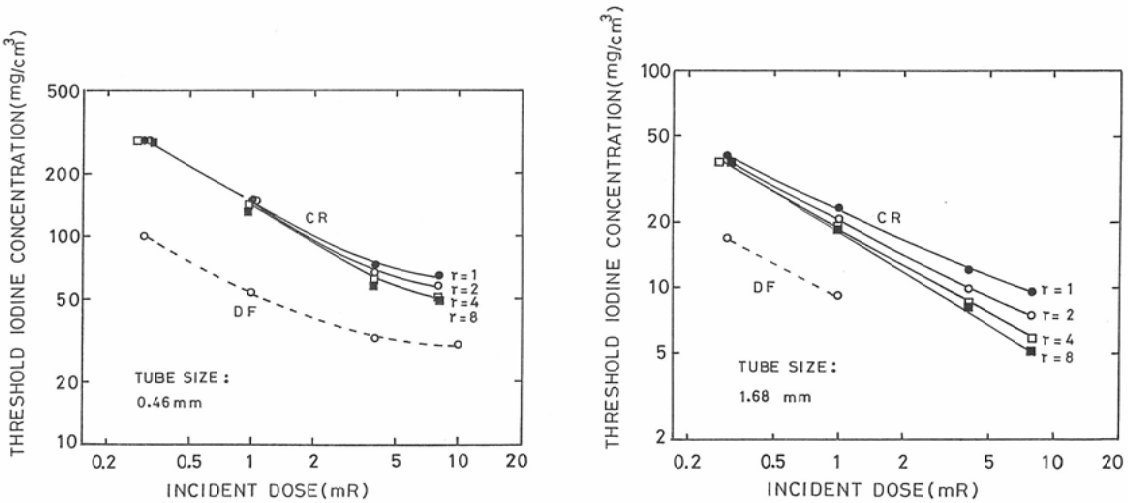

Fig. 5 Dependence of threshold iodine concentrations of 0.46-mm (a) and 1.68-mm (b)-diameter vessels on incident exposure for various overall contrast enhancement factors. In each figure, the four upper curves (solid curves) and the lowest curve (dashed curve) were obtained with the CR system and the DF system, respectively.

various incident exposures (Fig. 4). Within the range of incident exposures shown in Fig. 4, the threshold iodine concentration for a given vessel diameter decreases with increasing incident exposures and for a given threshold iodine concentration, the detectable vessle diameter decreases with increasing incident exposures. It is important to note that the effect of overall contrast enhancement is demonstrated in Fig. 4. For example, at the higher incident exposures (4 and 8 mR), the threshold iodine concentrations of the original signals obtained with the CR system are reduced significantly when the overall contrast enhancement factor of 4 is used. However, there was no significant reduction with the lower incident exposures (0.3 and 1 mR), with the exception of larger vessels.

(3) The dependence of detectability of simulated vessels on the incident exposure is demonstrated in relation to the threshold iodine concentrations in two different diameter vessels (0.46 and 1.68 mm) for various overall contrast enhancement factors (Fig. 5a, 5b). The four upper curves in each figure were obtained with the CR system. The lowest curve in each figure was obtained with the DF system for comparison. Within the range of incident exposures used in this experiments, the slop of curves at the large diameter vessel (b) increases with the overall contrast enhancement factor. On the other hand, no significant differences are observed among the threshold iodine concentrations of the small diameter vessel (a). It is important to note that the DF system yields improved detectability of simulated vessels over the CR system at the same incident exposures.

(4) Effects of overall contrast enhancement on the detectability of simulated vessels at two different incident exposures (0.3 and 8.0 mR) are demonstrated on C-D diagrams (Fig. 6). Little improvement is found in detectability by overall contrast enhancement regardless of the vessle diameters at the low incident exposure but the increase is evident at the hight incident exposure.

(5) The relative threshold iodine concentration of a 1.68-mm-diameter vessel is plotted against the overall contrast enahncement factor for various incident exposures (Fig. 7). The relative threshold iodine concentration of 100 was defined as the threshold iodine concentration of a 1.68-mm-diameter vessel without overall contrast enhancement for each incident exposure. Whithin the range of incident exposures

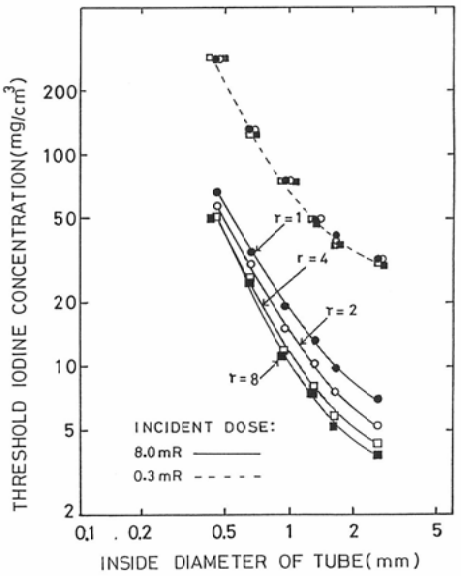

Fig. 6 C-D diagrams obtained with the CR system at incident exposures of 0.3 mR and 8 mR for various overall contrast enhancement factors.

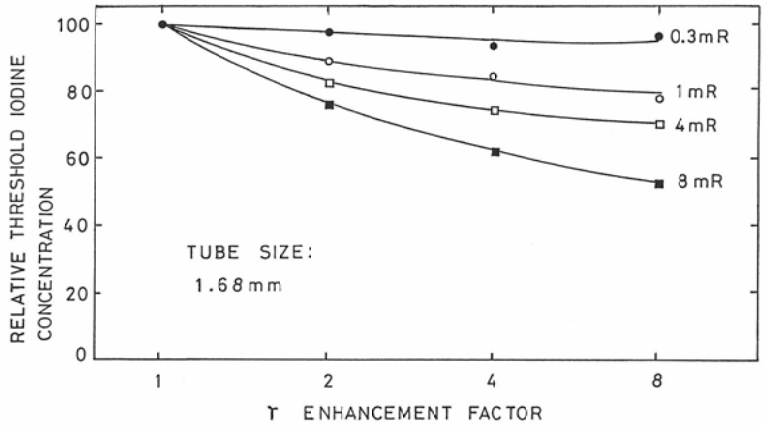

Fig. 7　Dependence of relative threshold iodine concentration of a 1.68-mm-diameter vessel on overall contrast enhancement factor for various incident exposures in the CR system.

demonstrated in Fig. 7, the higher the incident exposures, the greater the slope of curves. It is evident that, for any given incident exposure, the relative threshold iodine concentration decreases with the contrast enhancements.

Discussion

According to our study, the detectability of simulated vessels in CR images improved with increasing incident exposures.

The magnitude of quantum noise of the CR system was estimated by measuring the root-mean-square (RMS) noise of DSA images that were radiographed under the wide range of x-ray exposures.

In the range of low incident exposures, the RMS noise increased rapidly with decreasing incident exposures, indicating that contributions of the quantum noise were dominant. On the other hand, the RMS noise decreased and became nearly constant with increasing incident exposures in the range of high incident exposures, suggesting dominances of the structure noise of the IP and the other noise sources. It has been concluded from this result that the improvement in detectability by increasing incident exposures is mainly due to a decrease in the quantum noise.

The effect of overall contrast enhancements on the detectability of simulated vessels was studied in the CR system. The detectability of simulated vessels in CR images was improved significantly by overall contrast enhancement at the high incident exposures and the larger diameter vessels. With overall contrast enhancements, both the signal and the image noise are increased by the same factor, but the relative contribution of the human observer's internal noise[17][18] to the overall noise may be reduced, thus improving the detectability of the signal. The relative detectabilities of the large vessel (1.68 mm in diameter), except for the low incident exposure (0.3 mR), increased rapidly when the overall contrast enhancement factor increased from 1 to 2, but the increase was small when the factor was further increased. This result implies that excessive increase of contrast enhancement factor is less effective on the improvement in detectability. The contrast enhancement factor of 4 appears to be large enough to increase detectability nearly to its upper limit. Similar results were reported by Ishida et al.[17] in their observer performance studies of simulated low-contrast objects by using an 18-alternative forced-choice (18-AFC) method.

The reusltant C-D diagram obtained with the DF system indicated that the DF system yielded improved detectability of simulated vessels over the CR system at the same exposures incident on the

detectors.

We have measured the relative speed of the IP for its instanteneously emitted light by comparing the speeds of conventional screens. We found that the large amount of x-ray energy absorbed into the IP was emitted instantaneously prior to scanning with the laser beam.

In this study, an aluminum gird is placed before the IP of the CR system and a CFRP grid is attached to the II of the DF system. The incident exposures shown in this study have been measured in front of these grids for two systems. The x-ray transmission of the grid was 50% of an aluminum grid and 75% of a CFRP grid, respectively[19]. Therefore it is assumed that, the actual exposure incident on the II is greater than that incident on the IP by a factor of 50%, even when the x-ray exposure incident on each grid has been equivalent. These facts may be related to the superiority of the DF system in detectability of simulated vessels.

Furthermore, the other factors, such as differences in x-ray absorption and x-ray-to-light conversion efficiencies between the IP and the II, may be related to the difference in detectability of simulated vessels between two systems, though these points were not explored in this study.

In conclusion, DF system provides improved detectability of simulated vessles over CR system at the same incident exposures. The threshold iodine concentrations for detection of simulated vessels decreased with increasing object size and incident exposure. By overall contrast enhancement, detectability of simulated vessels obtained with CR system improved. However, the magnitude of improvement factor depends on the size of vessles and the incident exposures used.

Acknowledgements

The author gratefully acknowledges the careful experimental work of K. Morita, S. Doudanuki, N. Moribe, Y. Hirata, N. Katsuda and Y. Hiai. The author gratefully acknowledges useful discussions with T. Takada of the Kumamoto University Hospital during the performance of the experimantal study.

This work was supported by a grant-in-aid from the Japanese Ministry of Education.

References

1) Sonoda M, Takano M, Miyahara J, et al: Computed radiography utilizing scanning laser stimulated luminescence. Radiology, 148: 833—838, 1983
2) Sakurai K, Hachiya J, Korenaga T, et al: Digital radiography of the chest-Evaluation of normal anatomical structure and low dose radiography-. Nippon Act. Radiol. 44: 11—22, 1984
3) Nishitani H, Umezu Y, Ogawa K, et al: Dual-energy projection radiography using condenser x-ray generator and digital radiography apparatus. Radiology, 161: 533—535, 1986
4) Ishigaki T, Sakuma S, Horikawa Y, et al: One-shot dual-energy subtraction imaging. Radiology, 161: 271—273, 1986
5) Fajardo LL, Hillman BJ, Hunter JB, et al: Excretory urography using computed radiography. Radiology, 162: 345—351, 1987
6) Korenaga T, Hachiya J, Sakurai K, et al: Digital subtraction angiography (DSA) by Fuji computed radiography (FCR) system. Housyasenka, 2: 61—70, 1983
7) Uchino A, Hasuo K, Tamura S, et al: Cerebral angiography using Fuji computed radiography (FCR) system: Low exposure dose and diluted contrast material. Journal of Medical Imagings, 5: 1222—1225, 1985
8) Ihibashi T: Digital subtraction angiography (DSA) using Fuji computed radiography (FCR). Nippon Act. Radiol. 45: 1351—1376, 1985
9) Kudo S: Digital subtraction angiography with scanning laser stimulated luminescence; Experimental and clinical evaluations and comparisons with digital fluorography and conventional angiography. Nippon Act. Radiol, 45: 1503—1516, 1985
10) Nitatori T, Hachiya J, Korenaga T, et al: Whole body intravenous digital subtraction angiography. Radiology, 156: 829—830, 1985
11) Kamiya M, Takahashi F., Tsuneoka M, et al: High resolution digital subtraction system. Proc. SPIE, 626: 366—372, 1986

12) Fujita H, Doi K, Chan HP, et al: Dynamic and static phantoms for evaluation of digital subtraction angiographic systems. Radiology, 155: 799—803, 1985
13) Cohen G, DiBianca FA: The use of contrast-detail-dose evaluation of image quality in a computed tomographic scanner. Journal of computer assisted tomography, 3: 189—195, 1979
14) Cohen G: Contrast-detail-dose analysis of six different computed tomographic scanners. Journal of computer assisted tomography, 3: 197—203, 1979
15) Cohen G, Wagner LK, Amtey SR: Contrast-detail-dose and dose efficiency analysis of a scanning digital and a screen-film-grid radiographic system. Med. Phys. 8: 358—367, 1981
16) Loo LN, Doi K, Ishida M, et al: An empirical investigation of variability in contrast-detail diagram measurements. Proc. SPIE, 419: 68—76, 1983
17) Ishida M, Doi K, Loo LN, et al: Digital image processing: Effect on detectability of simulated low-contrast radiographic patterns. Radiology, 150: 569—575, 1984
18) Ohara K, Chan HP, Doi K, et al: Investigation of basic imaging properties in digital radiography. 8. Detection of simulated low-contrast objects in digital subtraction angiographic images. Med. Phys. 13: 304—311, 1986
19) Higashida Y, Hirata Y, Katsuda N, et al: Physical properties of low-dose system (carbon fiber cassette, table top, antiscatter grid) in diagnostic radiology. Jap. J. Rad. Thech., Special Eddition, 434, 1986

平成2年5月25日